https://doi.org/10.1016/j.enconman.2018.08.073

Modeling of a novel SOFC-PEMFC hybrid system coupled with thermal swing adsorption for H_2 purification: Parametric and exergy analyses

Zhen Wu[1,2], Zaoxiao Zhang[2,*], Meng Ni[1,*]

[1]Building Energy Research Group, Department of Building and Real Estate, The Hong Kong Polytechnic University, Hong Kong, P.R. China

[2]School of Chemical Engineering and Technology, Xi'an Jiaotong University, Xi'an, P.R. China

*Corresponding author, Email: meng.ni@polyu.edu.hk(M Ni) zhangzx@mail.xjtu.edu.cn (Z Zhang)

Abstract: A novel hybrid system fueled with natural gas (NG), consisting of solid oxide fuel cell (SOFC), proton exchange membrane fuel cell (PEMFC) and gas processing (GP) subsystem for H_2 production and purification, is proposed and modeled in this paper. The combination of water gas shift (WGS) and thermal swing adsorption (TSA) methods is adopted to convert the syngas out from the SOFC into H_2 with high purity for subsequent use as a fuel in PEMFC for additional power generation. The parametric and exergy analyses show that the proposed hybrid system can achieve high energy conversion efficiency of approximately 64% and exergy efficiency of 61%, which are higher than some other fuel cell systems, such as reformer-PEMFC, standalone SOFC, SOFC-engine/gas turbine and SOFC-chemical looping hydrogen production. The waste heat recovery for driving the TSA reaction and the H_2 recirculation for the PEMFC are found to improve the net electricity efficiency by 3.24% and 9%, respectively. In addition, using TSA method instead of the traditional pressure swing adsorption (PSA) could improve the efficiency of the

SOFC-PEMFC hybrid system without increasing the exergy destruction. These results reveal that the novel hybrid system is a promising energy conversion system with high efficiency.

Keywords: Solid oxide fuel cell; Proton exchange membrane; Metal hydride; Exergy; High-efficiency.

Nomenclature

Abbreviation

CLHP	chemical looping hydrogen production
DC/AC	direct current to alternating current
DIR	direct internal reforming
FC	fuel cell
GT	gas turbine
GP	gas processing
HEX	heat exchanger
HSA	hydrogen storage alloy
HT-WGS	high temperature – water gas shift
LT-WGS	low temperature – water gas shift
MH	metal hydride
NG	natural gas
PEMFC	proton exchange membrane fuel cell
PSA	pressure swing adsorption
R-PEMFC	reform-PEMFC

TSA	thermal swing adsorption
WGS	water gas shift

29

30 Symbols

A_{cell}	fuel cell area, m^2
C_d	hydrogen desorption reaction rate constant, s^{-1}
E_d	activation energy, J mol^{-1}
E_T^0	standard reversible voltage for H_2, V
Ex	exergy, kW
F	Faraday constant, C mol^{-1}
h	specific enthalpy, J mol^{-1}
$\frac{H}{M}$	hydrogen and metal atomic ratio
I	current, A
J	current density, A m^{-2}
K	reaction equilibrium constant
LHV_{fuel}	lower heating value of fuel, kW
M	molar mass, kg $kmol^{-1}$
n_{H_2}	hydrogen content, mol
P	power, kW
p	pressure, bar
Q_{loss}	heat loss of the fuel cell, kW
R_g	universal gas constant, J K^{-1} mol^{-1}

T	temperature, K
U_{ir}	irreversible voltage of the fuel cell, V
y	component concentration, mol L^{-1}
ϕ	mass flow, kg s^{-1}
μ_{fuel}	fuel utilization
η	energy efficiency
χ_{SOFC}	fuel recirculation percentage of SOFC
ζ	exergy efficiency
$\triangle H$	reaction enthalpy, J mol^{-1}

Subscript

a	anode
ab	absorption
AC	alternating current
AUX	auxiliary
c	cathode
cell	fuel cell
coolant	coolant
d	desorption
DC	direct current
eq	equilibrium
Gross	gross

H_2	hydrogen gas
H_2O	water
hfluid	heating fluid
in	inlet
ISE	isentropy
net	net
NG	natural gas
O_2	oxygen gas
ox	oxidant
out	outlet
ref	reference
reform	reforming
shift	water gas shift reaction
Steam	steam
Total	total
TSA	temperature swing adsorption
wfluid	working fluid

1. Introduction

Along with the upgraded living standard and rapid development of economics, the human needs for energy have been increasing day by day. A large-scale exploitation and utilization of traditional non-renewable energies have led to increasingly serious issues, such

as energy crisis and environmental pollution. Therefore, an efficient and clean energy utilization technology is a must for the sustainable development of society. Fuel cell (FC) power technology is attractive due to its high efficiency, diverse forms of application, low emission and noise [1-4]. Among the fuel cells, proton exchange membrane fuel cell (PEMFC) has relatively low operating temperatures (no more than 100℃), fast transient response and mature fabrication technology [5-7]. PEMFC is viewed to be a promising power generation technology. However, the PEMFC has to be fueled with pure hydrogen as the impurity such as CO can easily poison the Pt-based catalyst of PEMFC. Hydrogen source becomes a key issue for achieving the large-scale utilization of PEMFC. Unfortunately, an efficient, economical and safe hydrogen storage technology is still not available [8]. The most commonly used technology for hydrogen storage is traditional pressurized gas storage with extremely high operating pressure, which faces the challenges of security risk, low volumetric density and scarce infrastructure (e.g. hydrogen refueling station) [9,10]. These challenges significantly hinder the large-scale application of hydrogen energy system.

Unlike the PEMFC, the biggest merit of solid oxide fuel cell (SOFC) is wide choices of anode fuels, such as CH_4, biogas, natural gas (NG), petroleum gas and so on [11-13]. The poisonous CO for PEMFC can even be utilized as a fuel by SOFC for power generation. Compared with pure H_2, NG is much cheaper and widely available. Besides, high temperature SOFC fueled with NG could convert CH_4, the main component of NG, into H_2 by integrating direct internal reforming (DIR). The H_2 fuel can be delivered to the PEMFC for additional power generation. The combination of SOFC-DIR and PEMFC makes the fuel source transfer from pure H_2 to NG whose infrastructure (refueling station) is well-equipped

now. Therefore, more and more attentions have been drawn to the SOFC-PEMFC hybrid system. Dicks et al. [14] first evaluated the benefits of a system combining high- and low-temperature fuel cell types. It was found that the combined SOFC-PEMFC system using SOFC as a reformer for hydrogen production has a higher overall efficiency than the SOFC-only or reformer-PEMFC system. Rabbani et al. [15] further confirmed the overall efficiency of the combined SOFC-PEMFC system can be improved by 8%~16% compared with standalone SOFC or PEMFC system. Recently, Tan et al. [16] designed a hybrid power generation system consisting of SOFC and PEMFC and further performed a parametric optimization study on the hybrid system. However, the output syngas after the reforming reaction occurring in the SOFC, including H_2, CO, CO_2 and H_2O, is only treated with condensation process before entering into the downstream PEMFC. Actually, the impurity gases (CO, CO_2) of the mixture have a non-ignorable impact on the PEMFC performance due to the requirement of pure H_2. In order to improve the purity of H_2, Fernandes et al. [17] adopted the method of pressure swing adsorption (PSA) for H_2 separation to connect the reforming output and the PEMFC anode input in the hybrid system. Based on SOFC as a reformer to convert NG into H_2 for PEMFC, the authors proposed the innovative CaPP (Car as Power Plant) concept that the H_2 fuel from the SOFC reformer (SOFCR) is delivered into the PEMFC-powered car as the power plant to generate electricity when the car is in the parking situation.

The PSA technique is a completely physical separation process, based on the mechanism that different gases exhibit different behaviors under pressure changes [18]. Therefore, it is hard to obtain H_2 with very high purity from the reformed gas mixture (H_2, CO, CO_2 and

H_2O) by PSA. The H_2 purity processed by PSA is reported to be about 96% [19]. The existence of CO easily poisons the PEMFC catalyst, thus resulting in the FC performance degradation. This is because that the anodic Pt-based catalyst in the PEMFC only bears no more than 10 ppm of CO [20]. In contrast, thermal swing adsorption (TSA) is based on chemisorption at different temperatures to achieve H_2 separation and even purification. AB_5-type hydrogen storage alloy (HSA) is capable of separating and purifying H_2 from the gas mixture containing CO content up to 0.1% (volume percentage) [21]. The purity of the desorbed H_2 can reach as high as 99.9999% [22]. The pressure of H_2 fed into the PEMFC can be self-regulated by controlling the TSA temperature, while an extra compressor after the PSA process is needed to regulate H_2 pressure. In addition, the TSA chemical reaction based on HSA could be driven by waste heat recovery in the SOFC-PEMFC hybrid system. These benefits can potentially contribute to the improvement of energy conversion efficiency for the SOFC-PEMFC hybrid system.

To the best of our knowledge, no study on the SOFC-PEMFC hybrid system coupled with the TSA treatment for H_2 purification can be found from the literature. Therefore, the integrated system consisting of SOFC-DIR, WGS (water gas shift), TSA and PEMFC modules is proposed and modeled in the present study. Then, a parametric study is performed to analyze the influences of various important parameters on the performance of the hybrid system. Besides, detailed analyses of exergy flow and exergy loss of the main components in the hybrid system are carried out, which is significant for optimizing the hybrid FC system.

2. SOFC-PEMFC hybrid system coupled with TSA

Figure 1 shows the layout of the proposed hybrid system (labeled as SOFC-WGS-TSA-PEMFC). In this system, the NG fuel is first heated by the waste heat and then injected into the SOFC anode. Direct internal reforming reaction occurs in the SOFC, accompanying with the production and output of syngas (components in mole fraction: H_2O 44.38%, H_2 19.82%, CO 8.99%, CO_2 26.49% and N_2 0.32% in T_{reform}=1023 K). A part of syngas will be recycled back to mix with the fuel NG as a new fuel for SOFC anode. The remaining part of syngas keeps going on and plays a role in preheating the fuel NG and air as heat source for improving the system efficiency. Meanwhile, the temperature of the syngas is reduced to the required temperature 350℃ where the high-temperature WGS reaction happens.

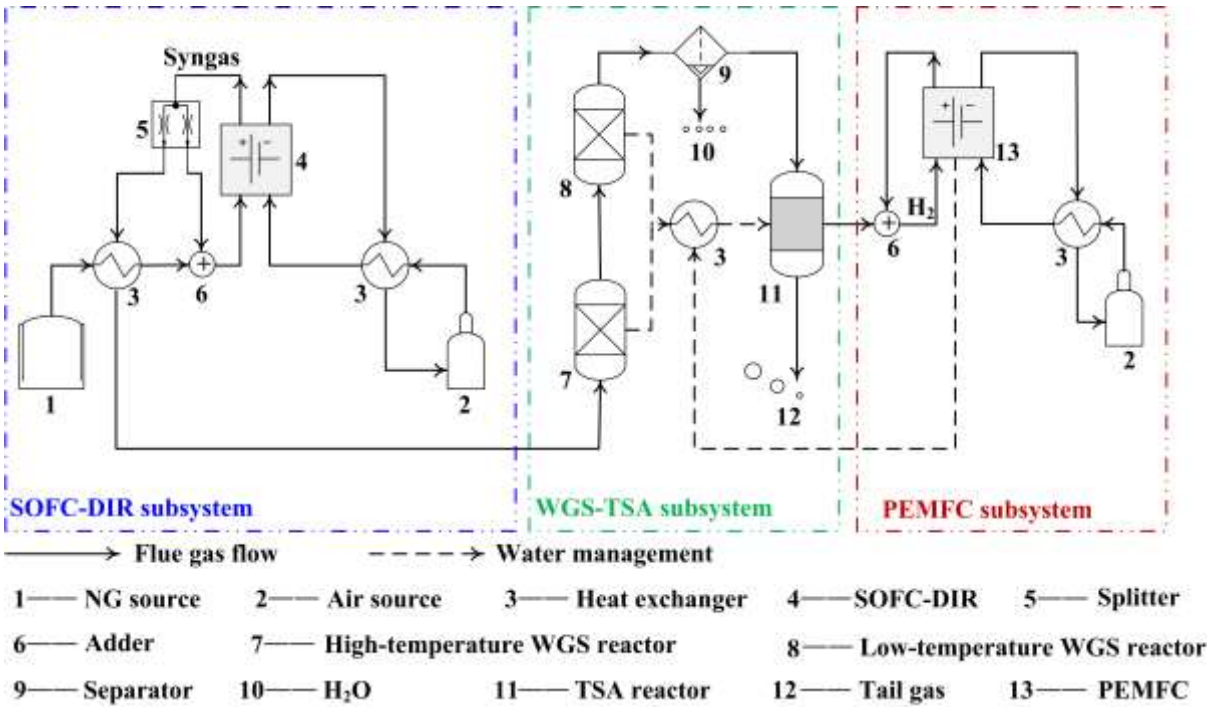

Fig. 1. The layout of the SOFC-WGS-TSA-PEMFC system.

In the gas processing (GP) subsystem consisting of WGS and TSA sections, the two stages WGS including high-temperature and low-temperature stages are adopted to ensure high converting rate and large H_2 production for the WGS reaction of the syngas. High-temperature WGS (HT-WGS) reaction makes high converting rate, while low-temperature WGS (LT-WGS) produces more H_2. The heat generated by WGS reaction is recycled to evaporate water and produce steam. After the WGS treatment, the syngas is cooled and dried prior to the TSA process. In the TSA process, only H_2 component of the syngas can be selectively adsorbed by AB_5-type HSA in chemisorption at room temperature to form MH (metal hydride). The other components of the syngas are exhausted to environment. When the MH reaction bed is heated to certain temperature (50~90℃), high pure H_2 is released from the MH to supply for the PEMFC as anode fuel. In order to improve the system net efficiency, the produced steam in the WGS process is used to heat the MH bed for driving hydrogen desorption reaction.

In the PEMFC subsystem, pure H_2 source separated from the TSA process is fed into the PEMFC. The unreacted H_2 in the PEMFC output is recycled back to the inlet for improving fuel utilization. Cathode air is heated by waste heat of tail gas to reach the required temperature prior to the input into the PEMFC. The cooling method using water as working medium is performed to make sure the operating temperature less than 100℃, preventing water from evaporating out of the PEMFC.

3. System model

3.1. Model assumptions

The following assumptions are made for simplifying the system model.

1) Pressure drops in the system are neglected.
2) The NG source with 3% H_2O is desulfurized.
3) The system is in steady-state operation.
4) High steam to carbon ratio is assumed in the SOFC where no carbon deposition is considered [23].
5) All the reactors (including the WGS and TSA reactors) and heat exchangers are assumed to be well insulated. There is no heat transfer between the devices (reactors and heat exchangers) and the outside environment.
6) The hydrocarbon component in the NG is assumed to completely convert into H_2 in the SOFC-DIR. The necessary heat required for the reforming reaction is taken from the electrochemical reaction in the SOFC. Besides, the reforming and WGS reactions in the system occur at the equilibrium temperature and pressure [24].
7) The modeling of SOFC-DIR is separated into the reforming and the electrochemical reactions. The gas fuel after the reforming reaction equilibrium is the input fuel of the subsequent electrochemical reaction. The local isothermal model is applied to fuel cell for calculating electrochemical balances based on the constant cell temperature [25].
8) The humidification of the PEMFC is not considered for the following reason. Our study only focuses on the stationary performance of the hybrid system. The humidification of flue gas has little influence on the efficiency and gas composition except increasing the humidity. Therefore, the reasonable simplification on the

PEMFC humidification is performed.

3.2. Models of the SOFC and PEMFC subsystem

The core of the SOFC subsystem shown in Fig. 2a is the SOFC fuel cell which works both as a NG reformer and a generator. The excessive air is input into the SOFC cathode for being used as the coolant to remove the generated reaction heat out of fuel cell, ensuring the isothermal operation of the SOFC. The internal reforming reaction, water gas shift reaction, and electrochemical reactions in the SOFC can be expressed in Eqs. (1-3) [26,27].

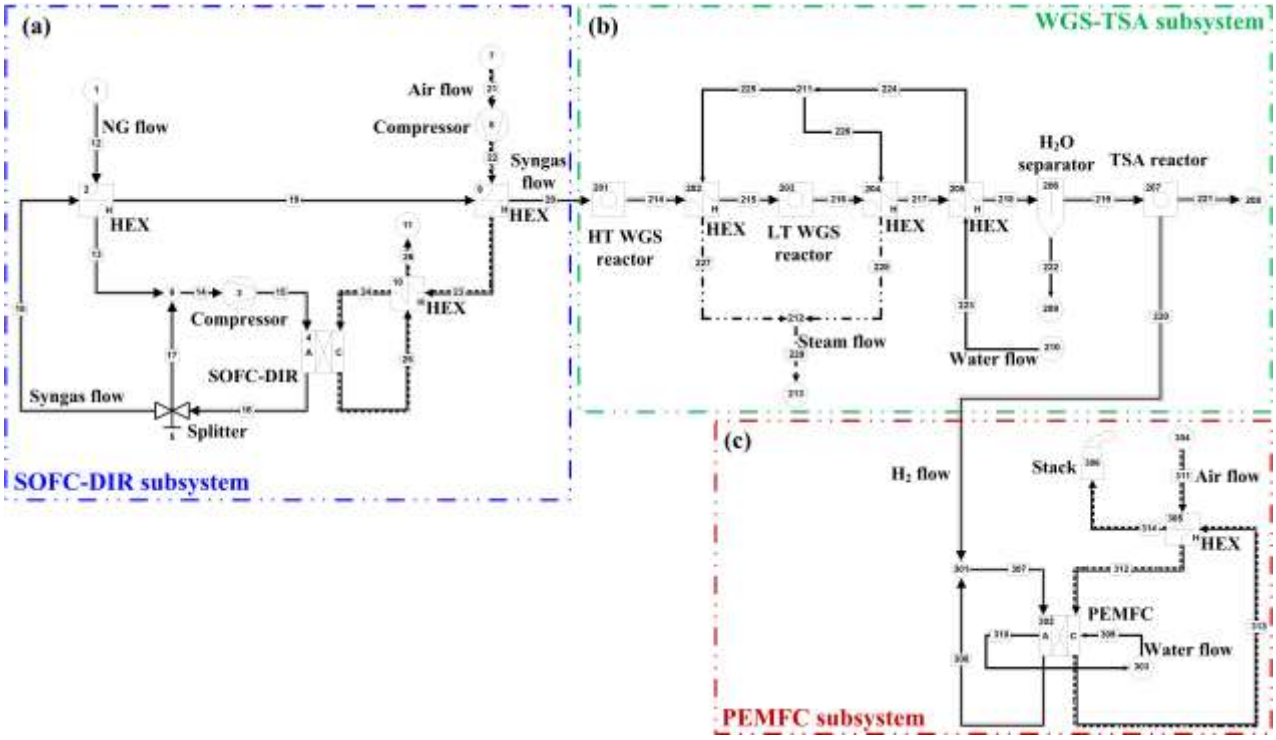

Fig. 2. The schematic model (a) SOFC subsystem; (b) WGS-TSA subsystem; (c) PEMFC subsystem.

$$CH_4 + H_2O \rightarrow CO + 3H_2 \quad \Delta H = 206 \text{ kJ/mol} \tag{1}$$

$$CO + H_2O \rightarrow CO_2 + H_2 \quad \Delta H = -41 \text{ kJ/mol} \tag{2}$$

$$H_2 + \frac{1}{2}O_2 \rightarrow H_2O(g) \quad \Delta H = -242 \text{ kJ/mol} \tag{3}$$

176 The reaction equilibrium constant K_{reform} of the reforming reaction occurring at the
177 equilibrium temperature T_{reform} can be described as below [28].

178
$$K_{reform} = \frac{p_{CO} \cdot p_{H_2}^{\ 3}}{p_{CH_2} \cdot p_{H_2O}} = f\left(T_{reform}\right) = -2.63121\times10^{-11} \cdot T^4 + 1.24065\times10^{-7} \cdot T^3 - 2.25232\times10^{-4} \cdot T^2 + 0.195028 \cdot T - 66.1395 \quad (4)$$

179 Figure 2 c shows the schematic model of the PEMFC subsystem. For the fuel cell (SOFC
180 and PEMFC) subsystems, the overall mass balance equation is described as follows.

181
$$\phi_{a,in} + \phi_{c,in} - \phi_{a,out} - \phi_{c,out} = 0 \quad (5)$$

182 The mass exchange between the anode and cathode in the fuel cells can be calculated by
183 Eq. (6).

184
$$\begin{aligned} \phi_{c\to a} &= \phi_{a,out} - \phi_{a,in} = M_{O_2} \cdot \frac{I}{4F} \quad \text{for SOFC} \\ \phi_{a\to c} &= \phi_{c,out} - \phi_{c,in} = M_{H_2} \cdot \frac{I}{2F} \quad \text{for PEMFC} \end{aligned} \quad (6)$$

185 The overall energy balance equation of the fuel cell is written as below.

186
$$\phi_{a,in} \cdot h_{a,in} + \phi_{c,in} \cdot h_{c,in} - \phi_{a,out} \cdot h_{a,out} - \phi_{c,out} \cdot h_{c,out} = P_{DC} + Q_{loss} \quad (7)$$

187 The relationship between anode mass flow $\phi_{a,in}$ and power output P of the fuel cell
188 can be described in the following equation.

189
$$\phi_{a,in} \cdot \mu_{fuel} \cdot \eta_{fuel} \cdot LHV_{fuel} = \frac{P}{\eta_{DC/AC}} = P_{DC} = A_{cell} \cdot J \cdot U_{ir} \quad (8)$$

190 The current density J can be calculated by Eq. (9). $y_{a,in,i}$ stands for the concentration
191 of the effective components involved with H_2 during the reforming and electrochemical
192 reactions.

193
$$J = \frac{I}{A_{cell}} = \frac{\mu_{fuel}}{A_{cell}} \cdot \frac{\phi_{a,in}}{M_a} \cdot \frac{\sum_i^n y_{a,in,i}}{2F} \quad (9)$$

Combining Eqs. (8) and (9), the relationship between power output P and fuel utilization μ_{fuel} could be obtained and described in Eq. (10).

$$P = \eta_{DC/AC} \cdot I \cdot U_{ir} = \mu_{fuel} \cdot \frac{\phi_{a,in}}{M_a} \cdot \frac{\sum_i^n y_{a,in,i}}{2F} \cdot \eta_{DC/AC} \cdot U_{ir} \tag{10}$$

The relationship between irreversible cell voltage U_{ir} and cell equilibrium conditions (cell pressure p_{Cell} and temperature T_{cell}) is shown as below. The third term in Eq. (11) represents the voltage loss ΔU_{loss} caused by the polarization under the assumption that the voltage loss over the length of the electrodes (the direction of the fuel flow) is ignored. For sake of simplicity, the voltage loss ΔU_{loss} is assumed to conform to Ohm's Law and equivalent to the local current density times a constant resistance R_{eq}. The values of R_{eq} and A_{cell} are obtained through the calculation under the design conditions of cell voltage U_{ir} and current density J.

$$U_{ir} = E_T^0 + \frac{R_g \cdot T_{cell}}{2F} \cdot \ln\left[\left(\frac{y_{c,O_2}^{1/2} \cdot y_{a,H_2}}{y_{a,H_2O}}\right) \cdot p_{cell}^{1/2}\right] - I \cdot R_{eq} \tag{11}$$

3.3. Model of gas processing subsystem

Figure 2 b shows the schematic model of the GP subsystem which contains two important reactors of WGS and TSA. In the WGS reactor, the water gas shift reaction occurs at the equilibrium temperature T_{react}. The equilibrium constant K_{shift} corresponding to the WGS reaction is the function of T_{react} as expressed in Eq. (12) [29].

$$\begin{aligned} K_{shift} &= \frac{p_{CO_2} \times p_{H_2}}{p_{CO} \times p_{H_2O}} = f\left(T_{WGS}\right) \\ &= 5.47301 \times 10^{-12} \cdot T^4 - 2.57479 \times 10^{-8} \cdot T^3 + 4.63742 \times 10^{-5} \cdot T^2 - 0.03915 \cdot T + 13.2097 \end{aligned} \tag{12}$$

In the TSA reactor, the AB_5-type HSA $LaNi_{4.3}Al_{0.7}$ against CO impurity [21] is used to complete the hydrogen absorption/desorption processes. The TSA reaction for hydrogen

separation and purification based on HSA can be described as Eq. (13). The hydrogen absorption/desorption reaction enthalpy of $LaNi_{4.3}Al_{0.7}$ alloy is $\Delta H = -29.2$ kJ/mol H_2 [30].

$$LaNi_{4.3}Al_{0.7} + 3H_2 \leftrightarrow LaNi_{4.3}Al_{0.7}H_6 \quad (13)$$

The TSA reaction takes place at the equilibrium pressure P_{eq} which is closely associated with the reaction temperature T_{react}. The relationship between P_{eq} and T_{react}, called as pressure-concentration isotherm, can be expressed in Eq. (14). The polynomial function coefficients a_n [31] are different for hydrogen absorption/desorption processes, which are listed in Table 1. The hydrogen desorption reaction kinetics of TSA can be written in Eq. (15) [32]. The main parameters of this equation are shown in Table 2.

$$p_{\mathrm{eq}} = \sum_{n=0}^{9}\left[a_n \cdot \left(\frac{H}{M}\right)^n \right] \cdot \exp\left[\frac{\Delta H}{R_g} \cdot \left(\frac{1}{T_{react}} - \frac{1}{T_{ref}} \right) \right] \quad (14)$$

$$\frac{dH}{dt} = C_d \cdot \exp\left(-\frac{E_d}{R_g T_d}\right) \cdot \left(\frac{p_g - p_{eq}}{p_{eq}} \right) \cdot H \quad (15)$$

Table 1 The polynomial function coefficients for hydrogen absorption/desorption [31].

Coefficient	a_0	a_1	a_2	a_3	a_4	a_5	a_6	a_7	a_8	a_9
Absorption	0.0075	15.2935	-34.577	39.9926	-26.7998	11.0397	-2.8416	0.446	-0.0391	0.0014
Desorption	-1.4654	19.1902	-42.086	49.0869	-33.8194	14.4375	-3.8581	0.6275	-0.0567	0.0021

Table 2 The main TSA reaction parameters.

Parameter	Value	Ref
Desorption rate constant, C_d (s^{-1})	9.57	[33]
Activation energy, E_d (J/mol)	23879.6	[31]
Reactor gas pressure, p_g (bar)	0.085	[31]
Absorbed hydrogen content, H (wt%)	0.7	[21]

3.4. Computational details

In the present study, Cycle-Tempo software, an elaborate thermodynamic system simulator designed by Delft University of Technology (TU Delft) [34], is used to perform thermodynamic modeling and exergy analysis for optimizing the SOFC-WGS-TSA-PEMFC system. The FC modular in the Cycle-Tempo was developed by A de Groot [25], which is capable of simulating almost all different types of fuel cells including SOFC and PEMFC. The Cycle-Tempo software has been successfully applied in the energy system optimization, which is proven to be a feasible and reliable tool for the stationary modeling and simulation [35-37]. During the calculations, the relative accuracy for the iteration operation is set as 1.0×10^{-4}. The counter-flow between fuel and air flows is chosen for the fuel cell. The values of the important input parameters used in the model computation are summarized in Table 3.

Table 3 Values of the important input parameters used in the model of the hybrid system.

Parameter	Value
Operating temperature of the SOFC, T_{SOFC} (K)	1023
Operating pressure of the SOFC, p_{SOFC} (bar)	1.013
Inlet temperature of fuel and air in the SOFC, $T_{in,SOFC}$ (K)	1023
Reforming reaction temperature in the SOFC, T_{reform} (K)	1023
Equilibrium pressure of the DIR reaction, p_{reform} (bar)	1.013
Outlet temperature of fuel and air in the SOFC, $T_{out,SOFC}$ (K)	1073
DC/AC conversion efficiency, $\eta_{DC/AC}$	0.96
Fuel utilization in the SOFC, $\mu_{fuel,SOFC}$	0.8
Cell voltage of SOFC, $U_{ir,SOFC}$ (V)	0.75

Current density, J (A/m^2)	2500
Isentropic efficiency of compressor, η_{ISE}	0.8
Fuel recirculation percentage of SOFC, χ_{SOFC}	0.4
Reaction temperature of HT-WGS, $T_{HT\text{-}WGS}$ (K)	623
Reaction temperature of LT-WGS, $T_{LT\text{-}WGS}$ (K)	473
Steam temperature, T_{Steam} (K)	383
Hydrogen absorption temperature of HSA, T_{ab} (K)	303
Hydrogen desorption temperature of MH, T_d (K)	353
Operating temperature of the PEMFC, T_{PEMFC} (K)	353
Operating pressure of the PEMFC, p_{PEMFC} (bar)	1.013
Inlet temperature of fuel and air in the PEMFC, $T_{in,PEMFC}$ (K)	353
Outlet temperature of fuel and air in the PEMFC, $T_{out,PEMFC}$ (K)	358
Cell voltage of PEMFC, $U_{ir,PEMFC}$ (V)	0.7
Fuel utilization in the PEMFC, $\mu_{fuel,PEMFC}$	0.85
Oxidant utilization in the PEMFC, $\mu_{ox,PEMFC}$	0.5
Temperature of cooling water, $T_{coolant}$ (K)	293

3.5. Model verification

Considering a steady state model discussed in this work, the energy balance of the model is calculated to perform the model verification. In this case, a random operating point of NG mass flow $\phi_{NG} = 0.06$ kg/s is chosen. The energy input and output of the SOFC-WGS-TSA-PEMFC system are summarized in Fig. 3. The energy input into the

system includes NG source, air source, heat source for TSA, water source and the consuming power of the auxiliary compressors. The one going out of the system has the power of fuel cells (SOFC and PEMFC), tail gas, steam, water out of the separator and the HEX cooling the PEMFC. The calculation compositions of gas flow and the energy results are shown in Table 4. The comparison between the input and output energy shows there is a small error of about 5.76 kW in the hybrid system. The very small relative error (about 0.33%) indicates the model verification of the SOFC-WGS-TSA-PEMFC system for the energy balance.

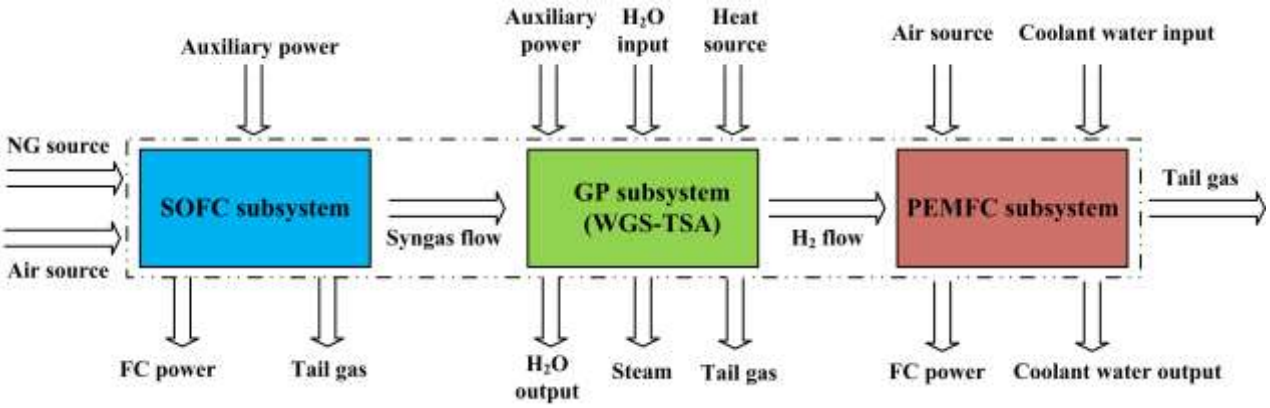

Fig. 3. The energy input and output of the SOFC-WGS-TSA-PEMFC hybrid system.

Table 4 The energy balance verification of the SOFC-WGS-TSA-PEMFC hybrid system.

		Components	Energy (kW)	Total energy (kW)	Error (kW)	Relative error
Input		NG source (CH_4: 85%, C_2H_6: 7%, C_3H_8: 2%, CO_2: 5%, N_2: 1%)	287.42	1723.15	5.76	0.33%
		Air source (N_2: 77.29%, O_2: 20.75%, CO_2: 0.03%, H_2O: 1.01%, Ar: 0.92%)	757.56			
		Heat source	-90.30			
	Water source	H_2O input in the GP	9.51			
		Coolant water input	886.97			
		Auxiliary power	-128.02			
	FC power	SOFC	1383.24			
		PEMFC	377.25			
Output	Tail gas	Gas out of SOFC (N_2: 80.52%, O_2: 17.44%, CO_2: 0.03%, H_2O: 1.05%, Ar: 0.96%)	-230.34	-1717.39		
		Gas out of TSA (CO_2: 98.74%, N_2: 1.14%, CO: 0.11%, CH_4: 0.01%)	-1356.40			
		Gas out of PEMFC (N_2: 70.02%, H_2O: 19.71%, O_2: 9.40%, Ar: 0.83%, CO_2: 0.03%)	-704.96			
		Steam	305.07			
	Water source	H_2O output in the GP	-899.06			
		Coolant water output	-592.19			

4. Results and discussion

4.1. SOFC-WGS-TSA-PEMFC system performance

The performance of the SOFC-WGS-TSA-PEMFC system is first predicted under the operating condition of SOFC output power $P_{SOFC} = 500\ \text{kW}$. The NG mass flow required to produce 500 kW and the corresponding H_2 mass flow produced from the GP subsystem are $\phi_{NG} = 0.022\ \text{kg/s}$ and $\phi_{H_2} = 0.002\ \text{kg/s}$, respectively. The output power of PEMFC depends on the H_2 production from the WGS reaction, which is calculated to be 129.80 kW. Therefore,

the generated total power of the fuel cells is $P_{Total} = P_{SOFC} + P_{PEMFC} = 629.80$ kW. In this case, the total energy of NG fuel input into the hybrid system is $E_{NG} = 926.10$ kW. The gross efficiency η_{Gross} of the hybrid system can be obtained to be 68.01% by Eq. (16), which is the ratio of total power P_{Total} to input NG fuel energy E_{NG}. Since some auxiliary power and thermal energy for TSA are consumed in the power generation process, this part of energy should be removed from the generated total power P_{Total}. Consequently, the net electricity efficiency η_{net} of the hybrid system is 60.46% when the SOFC output power is 500 kW under the given operating conditions. Table 5 lists the calculation results of the power generation and energy consumption in the hybrid system.

$$\eta_{Gross} = \frac{P_{Total}}{E_{NG}} \tag{16}$$

Table 5 The calculated power generation and efficiency of the hybrid system in the case of $P_{SOFC} = 500$ kW.

	Input energy (kW)	Total power (kW)		Auxiliary power (kW)		Thermal energy (kW)	Efficiency		
	NG fuel	SOFC	PEMFC	Compressor 3	Compressor 8	TSA reactor	Gross	Thermal	Net
Value	926.10	500	129.80	5.93	33.97	30.1	68.01%	3.24%	60.46%

It is of importance to note that the thermal energy $Q_{TSA} = 30.1$ kW required for the TSA process can be taken from the steam (Apparatus No.: 213) with the heat value $Q_{Steam} = 109.35$ kW generated by the WGS reaction through heat exchanger. The recovery of the heat source for driving the TSA reaction can improve the net electricity efficiency of the hybrid system by 3.24% to be 63.70%. Figure 4 shows the comparison of the overall

electricity efficiency among different fuel cell systems, such as Reformer-PEMFC (R-PEMFC) [38], standalone-SOFC [39], SOFC-CLHP [26], SOFC-engine [40], SOFC-GT [41] and SOFC-PEMFC hybrid system. It can be seen that the SOFC-PEMFC hybrid system has a higher efficiency than the other five kinds of fuel cell systems. The high energy conversion efficiency of the hybrid system indicates that the combination of SOFC and PEMFC contributes to the enhancement of energy conversion process besides the utilization of NG as fuel source. In addition, the coupling of TSA into the SOFC-PEMFC hybrid system causes an improved net electricity efficiency (63.70%) compared with the system coupled with PSA whose efficiency is 59.4% [17].

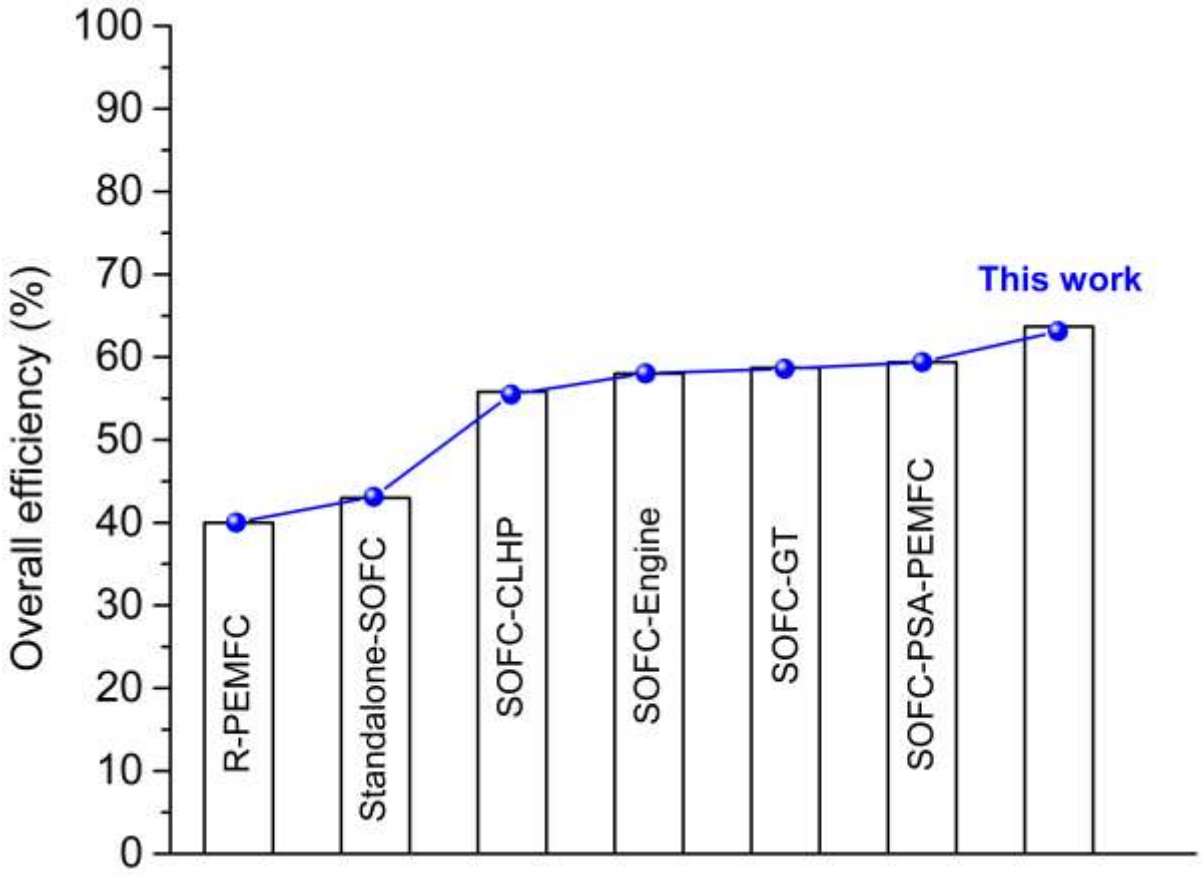

Fig. 4. The comparison of overall efficiency among different fuel cell systems [17,26,38-41].

4.2. Parametric analysis

The influences of some important operating parameters on the performance of the SOFC-WGS-TSA-PEMFC system are further investigated in this study. As is well known, the fuel utilization has a significant impact on the H_2 production and energy conversion efficiency. Therefore, the influences of fuel utilization on the H_2 production behavior, output power and net electricity efficiency of the hybrid system are first discussed. First, a set of SOFC fuel utilization $\mu_{fuel,SOFC}$=0.4, 0.5, 0.6, 0.7, 0.8 and 0.9 is considered under the same NG mass flow $\phi_{NG} = 0.022$ kg/s . Figure 5a shows the variations of H_2 production, the power generation and auxiliary power consumption with the increase of $\mu_{fuel,SOFC}$. It is found that increasing the SOFC fuel utilization can improve the SOFC power generation in an approximate linearity. According to Eq. (10) , the FC output power is proportional to the fuel utilization. Higher fuel utilization results in more power output generated by FC under the same operating conditions. Therefore, it is easily understood that the SOFC power generation increases with the increase of the SOFC fuel utilization. Meanwhile, more H_2 takes part in the electrochemical reaction to achieve more power at a higher $\mu_{fuel,SOFC}$. The consumption of H_2 in the SOFC causes the reduction in H_2 production occurring in the WGS reactors, accordingly reducing the power generation of PEMFC. Since the PEMFC power is much smaller than the SOFC power in the hybrid system, the total output power is mainly originated from the SOFC power. The fuel utilization $\mu_{fuel,SOFC}$ has a direct and more powerful impact on the SOFC compared with the PEMFC. Therefore, increasing $\mu_{fuel,SOFC}$ improves the total output power of the hybrid system, even though the PEMFC power generation is reduced. However, as shown in Fig. 5a, a small change appears in the total output power

when $\mu_{fuel,SOFC}$ is more than 0.7. In addition, the consumption of more H_2 in the SOFC caused by the higher $\mu_{fuel,SOFC}$ results in that the amount of air required to oxidize the increased H_2 in the fuel cell is increased. The increased air indicates more auxiliary power consumption of the compressor (Apparatus No.: 8). Taking the two influence factors of the large auxiliary power consumption and the small change in the total output power at a high $\mu_{fuel,SOFC}$ (more than 0.7) into account, the hybrid system with the high $\mu_{fuel,SOFC}$ has almost the same net electricity efficiency, about 63% shown in Fig. 5b. The net electricity efficiency reaches the maximum value 63.69% when the $\mu_{fuel,SOFC}$ is 0.8. Therefore, the SOFC fuel utilization will be fixed at 0.8 in the following study.

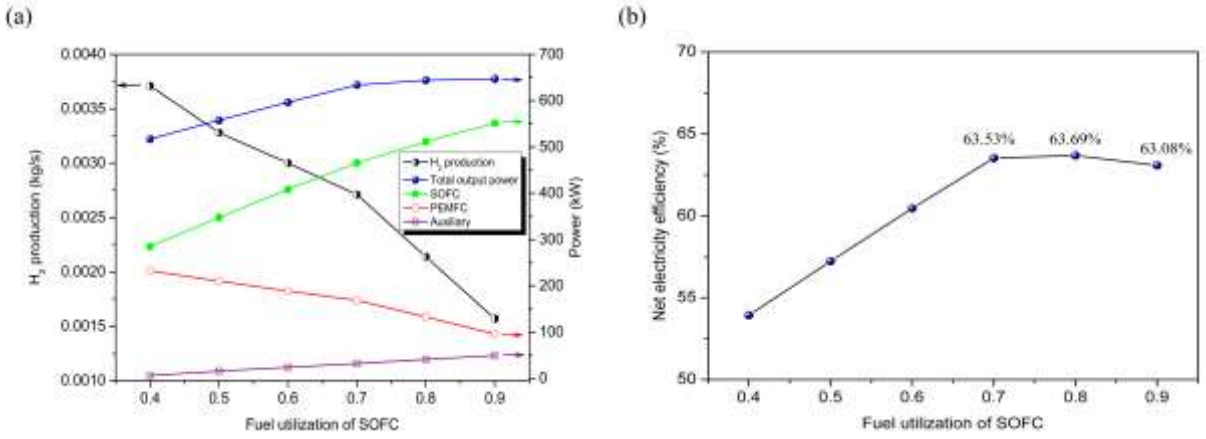

Fig. 5. The hybrid system performance at different SOFC fuel utilizations $\mu_{fuel,SOFC}$ (a) H_2 production and power; (b) net electricity efficiency.

Since the fuel of downstream PEMFC is pure H_2 from the WGS and TSA gas processing subsystem in the hybrid system, the PEMFC fuel utilization mainly affects the PEMFC power generation and the system net electricity efficiency. The SOFC power generation holds unchanged under the conditions of the fixed NG mass flow ϕ_{NG} and fuel utilization $\mu_{fuel,SOFC}$. Fig. 6 shows the variations of power generation and system efficiency with the increase of the PEMFC fuel utilization $\mu_{fuel,PEMFC}$ at $\phi_{NG} = 0.022$ kg/s and $\mu_{fuel,SOFC} = 0.8$. It can be seen that

both the power generation (PEMFC and total) and the net electricity efficiency are increased in a linear pattern when more H_2 fuel is consumed in the PEMFC. The overall efficiency of the hybrid system is increased from 55.28% to 62.28% when the $\mu_{fuel,PEMFC}$ varies from 0.4 to 0.9. If the recirculation of H_2 fuel out from the PEMFC outlet is considered, the $\mu_{fuel,PEMFC}$ will have no impact on the power generation and system efficiency. Because the H_2 fuel from the gas processing subsystem is completely consumed in this case. The total output power and efficiency of the hybrid system reach the stable values of 644.28 kW and 63.69%, respectively. Compared with the case without H_2 recirculation at $\mu_{fuel,PEMFC} = 0.4$, the efficiency under the H_2 recirculation can be improved by about 9%. Therefore, it is suggested to consider the H_2 recirculation for the PEMFC in the hybrid system with the purpose of improving the overall system efficiency.

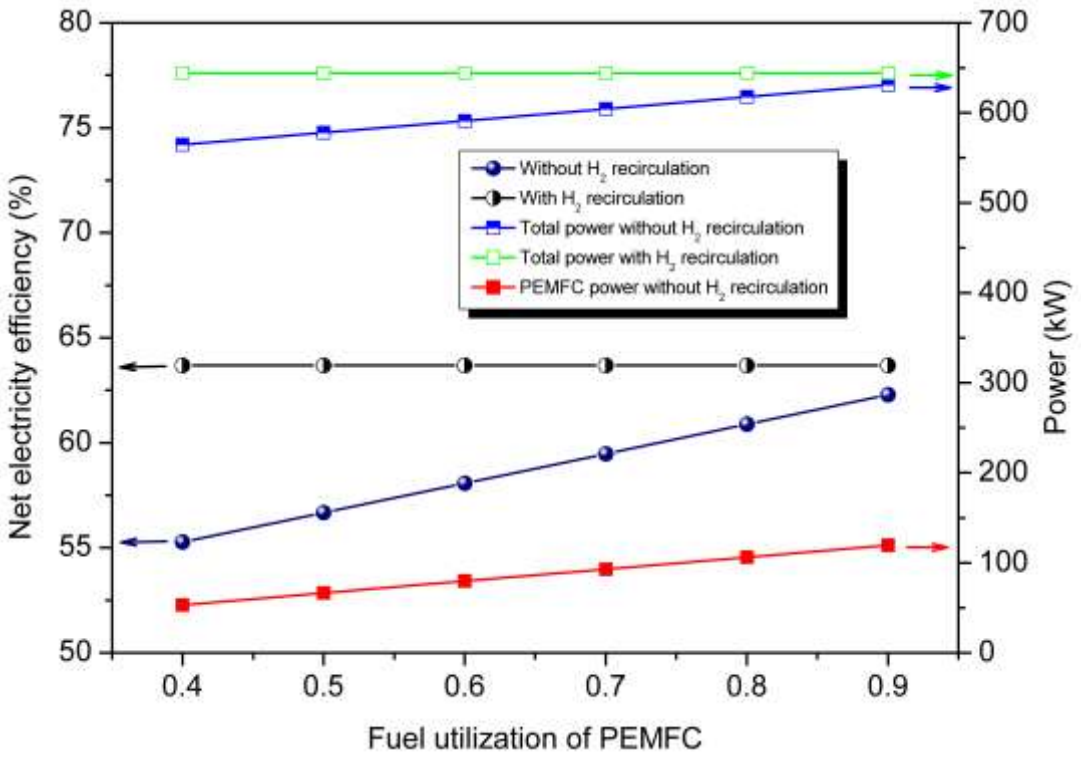

Fig. 6. The hybrid system performance with/without the H_2 recirculation at different PEMFC fuel utilizations $\mu_{fuel,PEMFC}$.

Figure 7 displays the influences of SOFC outlet syngas recirculation on the net electricity efficiency and power of the hybrid system. The recirculation χ_{SOFC} not only affects the performance of the SOFC, but also plays a crucial role on the subsequent H_2 production and the performance of the PEMFC. Increasing the χ_{SOFC} helps to enhance the SOFC performance, while overlarge χ_{SOFC} makes few H_2 produced from the WGS reaction and causes the performance degradation of the PEMFC as a result. The balance point of χ_{SOFC}, determining the best efficiency to the hybrid system, is found to be about 0.4, which agrees well with the reported conclusion that the FC hybrid system fueled with renewable fuels has the highest electricity efficiency with the syngas recirculation percentage of 40% [42].

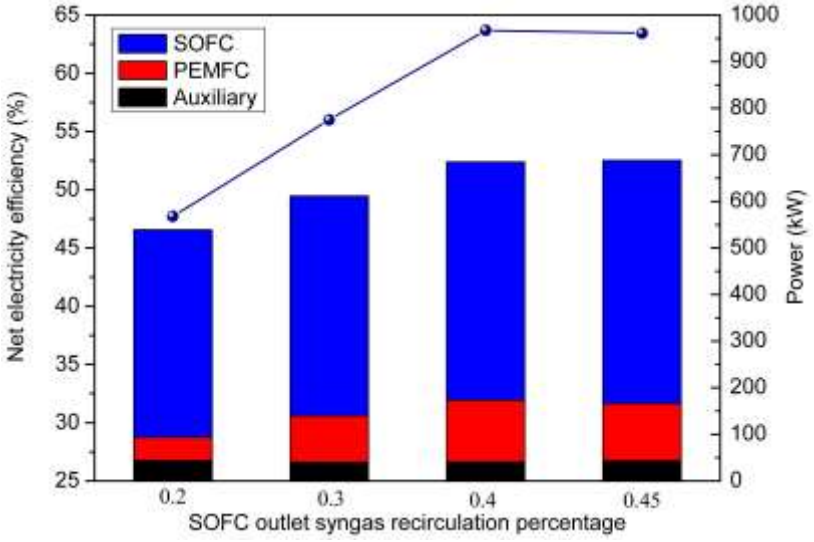

Fig. 7. The influences of χ_{SOFC} on the net electricity efficiency and power of the hybrid system.

The influences of operating temperatures on the performance of the hybrid system are further investigated in this work. Since the CH_4 reforming reaction is internally coupled into the SOFC, the operating temperature of the SOFC is supposed to be also the reforming reaction temperature. Figure 8a shows the performance of the hybrid system at different reforming temperatures of T_{reform}= 923, 973, 1023, 1073, 1123, 1173 and 1223 K under the

optimal fuel utilization conditions ($\mu_{fuel,SOFC}$=0.8 and χ_{SOFC}=0.4) and fixed current density J_{SOFC}=2500 A/m^2. As the T_{reform} increases, the power generation of SOFC decreases. The reduction in the SOFC power is attributed to the decrease of H_2 production in the SOFC-DIR, because the reforming reaction constant K_{shift} is reduced at the elevated reforming operating temperature. It means that the amount of H_2 fuel produced from the reforming reaction for electrochemical reaction in the SOFC-DIR is reduced at the elevated T_{reform}. As a consequence, the amount of the syngas from SOFC anode outlet is increased. On the contrary, the H_2 fuel produced from the syngas after the two-stage WGS and TSA processes is increased, which is from 0.00139 to 0.00226 kg/s with the increase of T_{reform} from 923 to 1223 K. Therefore, the PEMFC power increases with the increase of T_{reform}. The auxiliary power (mainly the compression power for air and H_2 sources) also becomes large at the elevated T_{reform}, because more compression work is required to achieve the higher fuel inlet temperature. In a word, the total output power of the hybrid system first increases and then decreases as the reforming temperature is increased. The net electricity efficiency of the hybrid system reaches the peak value of 63.32% at the T_{reform} of 1023 K.

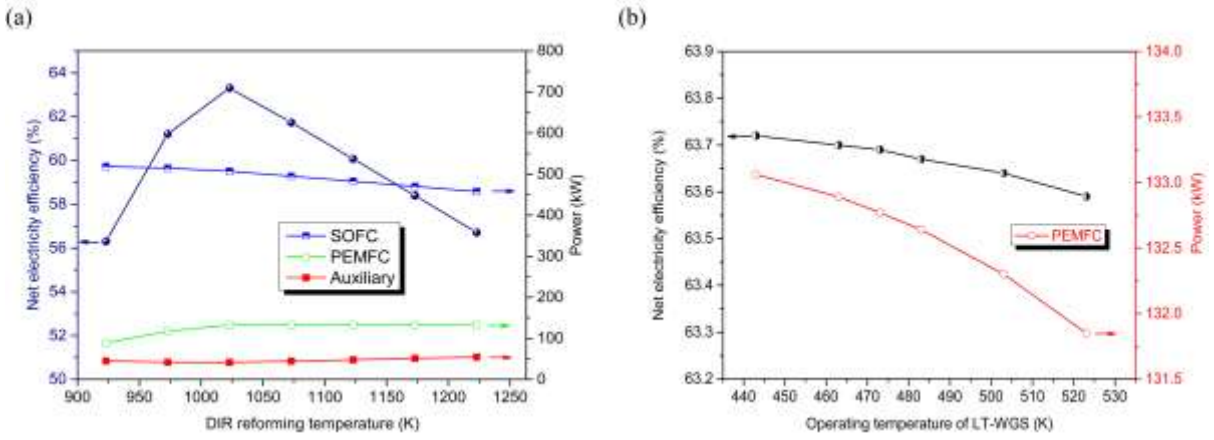

Fig. 8. The hybrid system performance at different operating temperatures (a) DIR reforming temperature; (b) LT-WGS operating temperature.

In order to achieve fast converting rate and high H_2 production in the WGS reactors, two-stage reactions with high and low temperatures are used in the gas processing subsystem. In view of H_2 production mainly depending on the LT-WGS reaction, the influence of LT-WGS operating temperature of 443~523 K on the hybrid system performance is studied. In this case, the operating temperature of the HT-WGS reaction is fixed at 623 K. As shown in Fig. 8b, the reduction in the LT-WGS operating temperature benefits for improving the PEMFC power generation and overall system efficiency. The enhanced PEMFC power indicates that the reduced LT-WGS operating temperature facilitates the H_2 production, as listed in Table 6. The mole fraction of H_2 component in the mixture gas after the LT-WGS reaction increases from 28.48% to 28.75% when the LT-WGS operating temperature is reduced from 523 K to 443 K. Accordingly, the H/C ratio of the mixture gas is incresed from 1.605 to 1.621. These results reveal that lower reaction temperature promotes the H_2 conversion reaction in the LT-WGS reactor and enriches the H_2 production as a result. In addition, the mole fraction of CO component in the mixture gas which is input into the TSA reactor based on $LaNi_{4.3}Al_{0.7}$ (HSA) is reduced with the decrease of LT-WGS reaction temperature. When the temperature is less than 463 K, the concentration of CO can be controlled below 0.1%, which is non-toxic to the HSA. Therefore, the control of LT-WGS reaction temperature is important to avoid CO component poisoning the TSA process. Although the reduced LT-WGS reaction temperature has a positive influence on the hybrid system performance, the influence is weak. The operating temperature of 463 K is recommended for the LT-WGS to achieve the high overall system efficiency without CO poisoning.

Table 6 The H_2 and CO mole fractions and the H/C ratio in the mixture gas after the LT-WGS reaction at different temperatures.

Temperature	443 K	463 K	473 K	483 K	503 K	523 K
H_2 mole fraction	28.75%	28.71%	28.68%	28.65%	28.58%	28.48%
CO mole fraction	0.06%	0.10%	0.13%	0.16%	0.23%	0.33%
H/C ratio	1.621	1.618	1.616	1.614	1.611	1.605

In the SOFC-WGS-TSA-PEMFC system, the H_2 fuel injected into the PEMFC is from the hydrogen desorption of MH in the TSA reactor. The PEMFC operating temperature is self-regulated according to the hydrogen desorption temperature of TSA reactor, which suggests that the PEMFC and TSA reactor have the same operating temperature. According to Eq. (15), the H_2 production in the TSA reactor is closely associated with the hydrogen desorption temperature T_d. In other word, the PEMFC operating temperature affects the H_2 fuel mass flow fed into the PEMFC. Figure 9 shows the influences of the PEMFC operating temperature on the performance of the hybrid system. It can be seen that the relationship between equilibrium pressure and temperature is linear, which conforms to the Van't Hoff equation describing the variation of the equilibrium pressure with the reaction temperature for MH [43]. The higher the operating temperature is, the more the H_2 production is. Therefore, the PEMFC can generate more power at higher temperatures. Of course, the thermal energy supplied for the TSA reactor is also increased when increasing the temperature T_d. As previously mentioned, the steam heat can be utilized to cover this part of thermal energy. Thus, the increase of the required thermal energy has no influence on the net electricity

efficiency. However, the large H_2 fuel mass flow inevitably reduces the operating time of the PEMFC, because of the fixed total H_2 amount produced by the SOFC-DIR and WGS reactors. Consequently, the highest possible PEMFC operating temperature will not benefit for the overall performance of the hybrid system.

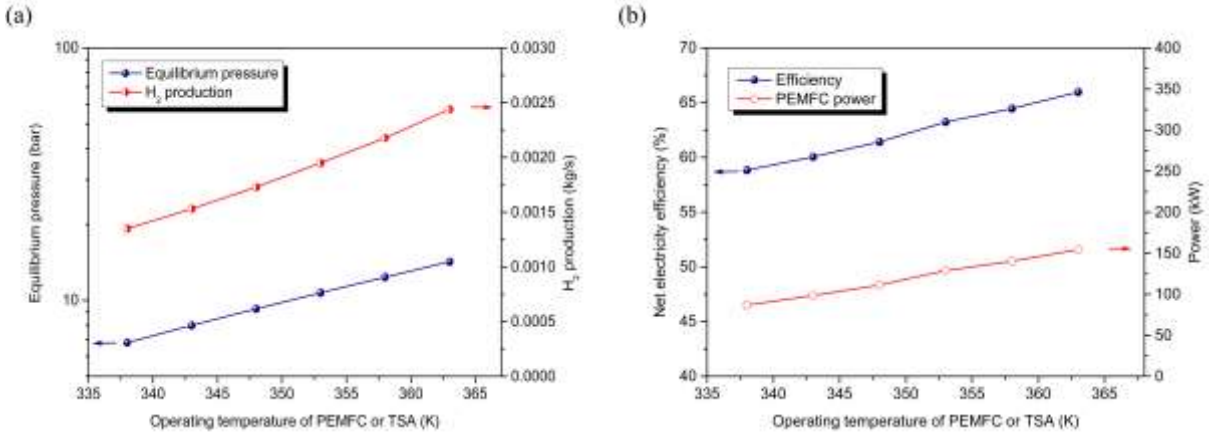

Fig. 9. The hybrid system performance at different PEMFC operating temperatures (a) H_2 production and equilibrium pressure; (b) net electricity efficiency and power.

4.3. Exergy analysis

The exergy analysis can help to find out which component of the system dominates the energy irreversibility of the whole system, thus providing the approach of optimizing the system performance. Therefore, the exergy analysis of the SOFC-WGS-TSA-PEMFC system is further performed under the same environment condition (1.013 bar and 288 K) in this paper. The results from the parametric analysis reveal that the novel hybrid system presents the superior performance when the important operating parameters are set as $\mu_{fuel,SOFC}$=0.8, χ_{SOFC}=0.4, T_{SOFC}=1023 K, $T_{LT\text{-}WGS}$=463 K, T_d=T_{PEMFC}=353 K and complete H_2 recirculation for the PEMFC. At the given optimum operation, the exergy flow and exergy efficiency of the hybrid system are calculated under the same NG fuel condition of $\phi_{NG} = 0.022$ kg/s .

Similar to the calculation equation of energy efficiency (Eq. (16)), the equation for the gross exergy efficiency can be written as the following equation. When calculating the net exergy efficiency, this part of exergy consumed by the auxiliary apparatus should be removed from the output exergy of the fuel cells.

$$\xi_{Gross} = \frac{Ex_{SOFC} + Ex_{PEMFC}}{Ex_{NG}} \quad (17)$$

Table 7 lists the calculation results of the output exergy Ex_{Total}, the input NG source exergy Ex_{NG}, the auxiliary exergy Ex_{AUX} and the corresponding exergy efficiency. The gross exergy efficiency of the hybrid system is 65.04%. The net exergy efficiency with the consideration of the heat source recovery for driving the TSA reaction (the thermal efficiency: 3.06%) is 60.89%.

Table 7 The calculated exergy and exergy efficiency of the hybrid system.

	Input exergy (kW)	Total power (kW)		Auxiliary power (kW)	Exergy efficiency	
	NG fuel	SOFC	PEMFC	Compressors	Gross	Net
Value	984.29	511.51	128.66	40.82	65.04%	60.89%

The exergy flow diagram in the SOFC-WGS-TSA-PEMFC system is shown in Fig. 10. In the hybrid system, a total exergy destruction of 39.09% occurs and the exergy efficiency of 60.91% is achieved. The exergy flow starts from the NG fuel source with $Ex_{NG} = 984.29$ kW and then enters into the SOFC-subsystem. In this subsystem, 22.38% of the exergy is destructed, which is the largest exergy destruction among the three subsystems. The PEMFC subsystem has the second largest exergy destruction which is 11.40%. Compared with the fuel cells subsystems, the GP subsystem has the smallest exergy destruction of 5.31%. The

results reveal that the subsystems involving fuel cells usually have the high exergy destruction. Actually, the exergy destruction in the H_2 separation and purification process is very small. The TSA process in this case is about 0.99%, which is comparable to the PSA process (0.8%) reported in the CaPP-SOFCR [17]. Besides, this part of the exergy can be supplied by the thermal utilization of the produced steam in the WGS reactor, indicating that the exergy destruction of TSA process can be recovered in our hybrid system. Therefore, the replacement of TSA for PSA process in the hybrid system has little influence on the exergy efficiency. Moreover, the SOFC-WGS-TSA-PEMFC hybrid system can prevent the gas impurity component CO from poisoning the PEMFC, which is conducive to long-cycle operation of the hybrid fuel cell system.

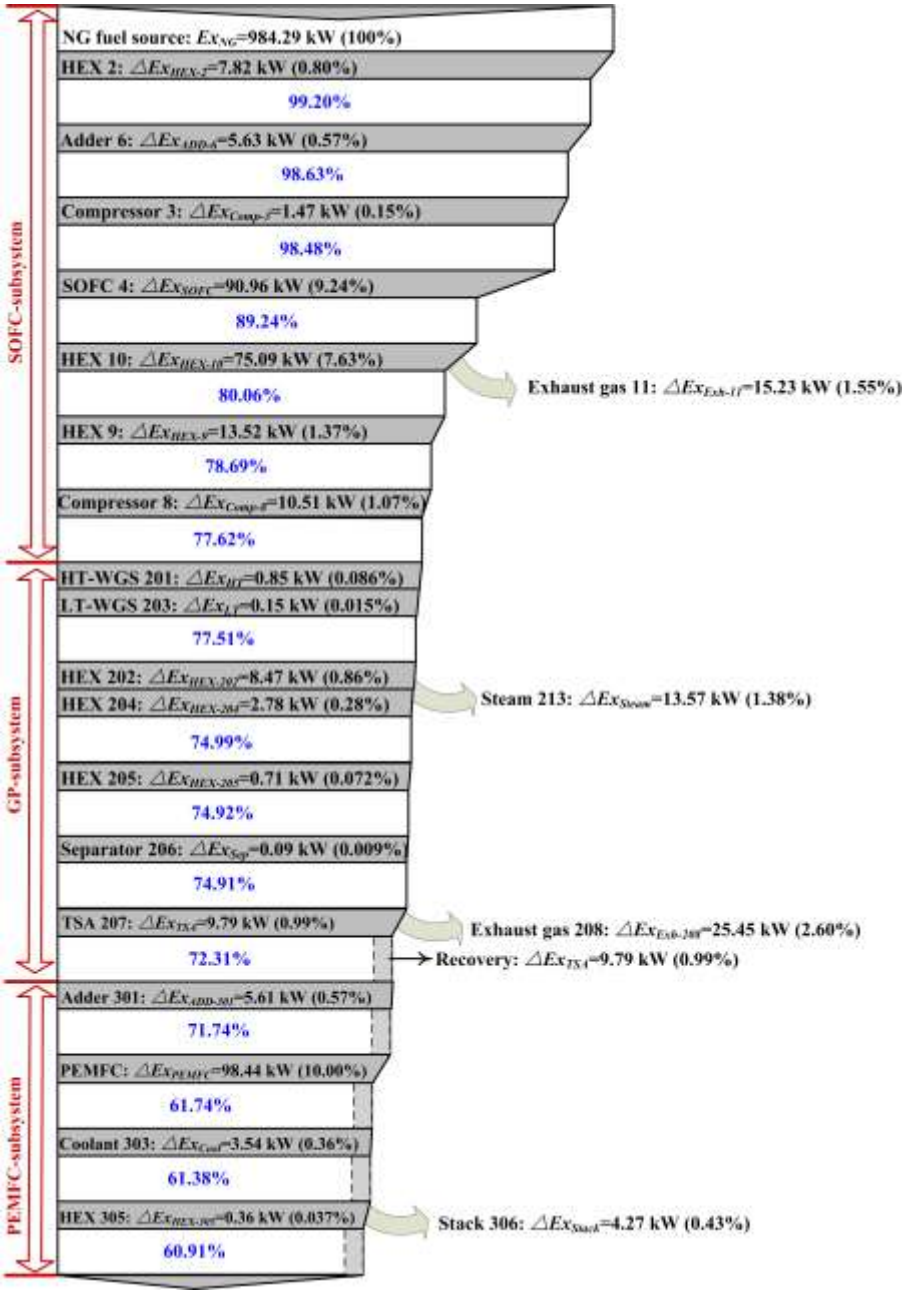

Fig. 10. Exergy flow diagram of the SOFC-WGS-TSA-PEMFC system.

Figure 11 displays the exergy loss of the components and the corresponding ratio to the total exergy loss in the SOFC-WGS-TSA-PEMFC system. In the SOFC subsystem, the SOFC-DIR component and the HEX component (Apparatus No.: 10) contribute a major part of exergy loss. The relative exergy loss (the ratio of exergy loss of each component to total system) of the two components reach up to 23.65% and 19.53%, respectively. For the SOFC-DIR, the high exergy loss is mainly attributed to the occurrence of the reforming and

electrochemical reactions. The reason for the high exergy loss of the HEX 10 component is a big temperature difference between the working fluid (air flow) and the heating fluid (exhaust gas flow from the SOFC-DIR cathode). The temperature of the air flow is increased from 318 K to 1023 K through the HEX 10 so that the air can be fed into the cathode of the fuel cell after the preheating. Meanwhile, the gas flow exhausted from the SOFC-DIR cathode is cooled down to about 355 K for venting to the environment. The waste heat recovery of the SOFC-DIR to preheat the air flow reduces the exergy loss of the exhaust gas flow to about 3.96%. Actually, the excessive heat of the syngas flow from the SOFC-DIR anode is also considered to preheat the NG fuel and the initial air flow in this case. However, the HT-WGS reaction with the syngas as the reactants is required to take place at a temperature as high as 623 K. The syngas heat out from the anode outlet that can be utilized for preheating is limited. In the HEX 9, the temperature of the working fluid (air flow) is increased by only 12 K (306 K to 318 K). This is also the reason why the HEX 10 has the big temperature difference between the working fluid and the heating fluid. In such a situation, the exergy efficiency of the HEX 9 is very low, which is calculated to be only 12.51% according to Eq. (18) [44]. By comparison, the exergy efficiency of the HEX 10 can reach up to 92.15%. The comparison confirms that the heat exchange is more in the HEX 10 than the HEX 9.

$$\xi_{HEX} = \frac{Ex_{wfuild,out} - Ex_{wfuild,in}}{Ex_{hfuild,in} - Ex_{hfuild,out}} \tag{18}$$

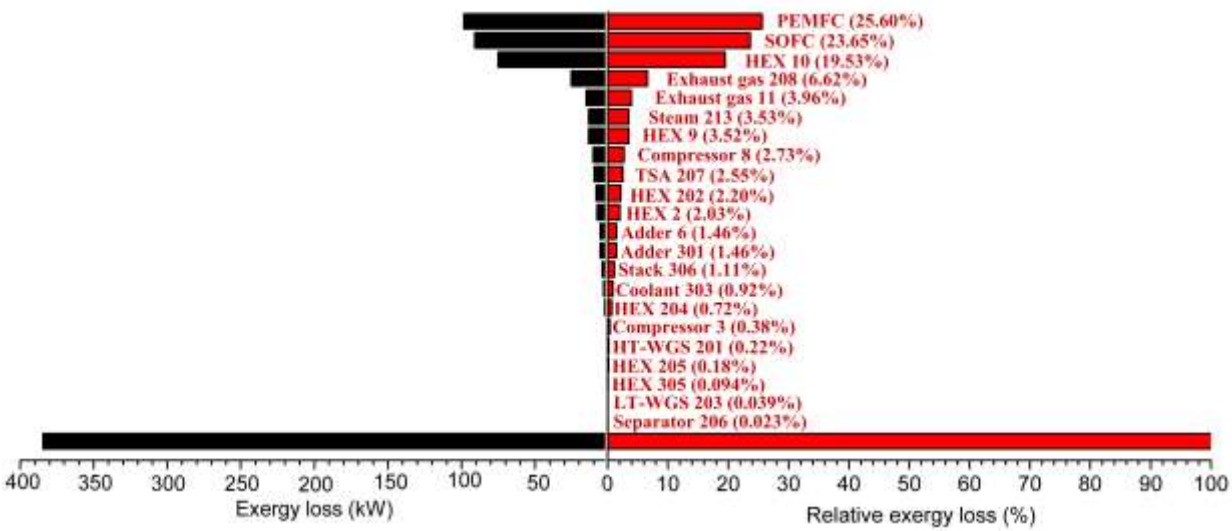

Fig. 11. Absolute and relative exergy loss of the main components in the SOFC-WGS-TSA-PEMFC system.

In the GP subsystem containing the WGS and TSA, the largest exergy loss is the exhaust gas (CO_2 of 98.8%) from the TSA reactor. The relative exergy loss of the exhaust gas is 6.62%. The largest exergy loss of the hybrid system appears in the PEMFC component. The relative exergy loss of the PEMFC reaches 25.60%. Actually, the exergy loss of the fuel cells SOFC and PEMFC dominates nearly 50% of the total exergy loss. Therefore, the exergy analysis further confirms that the fuel cells play an important role on determining the performance of the hybrid system.

5. Conclusions

In summary, a novel SOFC-WGS-TSA-PEMFC system fueled with NG is proposed and modeled in this paper. The parametric and exergy analyses are further performed and discussed to optimize the performance of the hybrid system. Through the analyses, the following conclusions can be drawn.

(1) The SOFC-WGS-TSA-PEMFC system presents a high net electricity efficiency up to about 64%, which is also more efficient than the reported R-PEMFC, only-SOFC, SOFC-CLHP, SOFC-engine and SOFC-GT fuel cell systems. In addition, the replacement of TSA for the PSA process to achieve H_2 separation and purification helps to improve the energy conversion efficiency of the SOFC-PEMFC hybrid system and prevent the PEMFC from being poisoned.

(2) The parametric analysis reveals that the optimum operating conditions for the hybrid system are $\mu_{fuel,SOFC}$=0.8, χ_{SOFC}=0.4, T_{SOFC}=1023 K, $T_{LT\text{-}WGS}$=463 K and T_d=T_{PEMFC}=353 K. The complete H_2 recirculation is suggested to the PEMFC for high efficiency. The LT-WGS reaction temperature should be controlled below 463 K to prevent CO component from poisoning the AB_5 type hydrogen storage alloy.

(3) The net exergy efficiency of the hybrid system under the optimal operating conditions can reach 60.91%. The SOFC and PEMFC components account for nearly half of the total exergy loss, indicating the dominant role in the hybrid system. Besides, the TSA process for H_2 separation and purification has the comparable exergy destruction to the PSA process, both of which are very small (less than 1%).

Acknowledgments

This work is partially supported by the Hong Kong Scholar Program (No. XJ2017023), the National Natural Science Foundation of China (No. 51506174) and the Natural Science Foundation of Shaanxi Province (No. 2017JQ5059).

References

[1] Xu HR, Chen B, Tan P, Zhang HC, Yuan JL, Irvine JTS, NI M, Performance improvement of a direct carbon solid oxide fuel cell through integrating an Otta heat engine, Energy Conversion and Management 2018, 165: 761-770.

[2] Zhang HC, Kong W, Dong FF, Xu HR, Chen B, Ni M, Application of cascading thermoelectric generator and cooler for waste heat recovery from solid oxide fuel cells. Energy Conversion and Management 2017; 148: 1382-1390.

[3] Ni M, Leung MKH, Leung DYC, Parametric study of solid oxide fuel cell performance. Energy Conversion and Management 2007; 48(5): 1525-1535.

[4] Xu HR, Chen B, Tan P, Cai WZ, He W, Farrusseng D, et al. Modeling of all porous solid oxide fuel cells. Appl Energy 2018;219:105–113.

[5] Ito H. Economic and environmental assessment of residential micro combined heat and power system application in Japan. Int J Hydrogen Energy 2016;41:15111–15123.

[6] Liu YF, Fan L, Pei PC, Yao SZ, Wang F. Asymptotic analysis for the inlet relative humidity effects on the performance of proton exchange membrane fuel cell. Appl Energy 2018;213:573–584.

[7] Budak Y, Devrim Y. Investigation of micro-combined heat and power application of PEM fuel cell systems. Energy Convers Manage 2018;160:486–494.

[8] Wu Z, Zhu LY, Zhang ZX, Yang FS, Wang YQ. DFT insights into the interactive effect of Ni+N cosubstitution on enhanced dehydrogenation properties of $Mg(BH_4)(NH_2)$-like complex hydride for hydrogen energy storage. J Phys Chem C 2018;122:5956–5966.

[9] Barthelemy H, Weber M, Barbier F. Hydrogen storage: Recent improvements and

563 industrial perspectives. Int J Hydrogen Energy 2017;42:7254–7262.
564 [10] Singh S, Jain S, Venkateswaran PS, Tiwari AK, Nouni MR, Pandey JK, et al. Hydrogen:
565 A sustainable fuel for future of the transport sector. Renew Sustain Energy Rev
566 2015;51:623–633.
567 [11] Baldinelli A, Barelli L, Bidini G, Di Michele A, Vivani R. SOFC direct fuelling with
568 high-methane gases: Optimal strategies for fuel dilution and upgrade to avoid quick
569 degradation. Energy Convers Manage 2016;124:492–503.
570 [12] D'Andrea G, Gandiglio M, Lanzini A, Santarelli M. Dynamic model with experimental
571 validation of a biogas-fed SOFC plant. Energy Convers Manage 2017;135:21–34.
572 [13] Buonomano A, Calise F, d'Accadia MD, Palombo A, Vicidomini M. Hybrid solid oxide
573 fuel cells – gas turbine systems for combined heat and power: A review. Appl Energy
574 2015;156:32–85.
575 [14] Dicks AL, Fellows RG, Mescal CM, Seymour C. A study of SOFC-PEM hybrid systems.
576 J Power Sources 2000;86:501–506.
577 [15] Rabbani A, Rokni M. Modeling and analysis of transport processes and efficiency of
578 combined SOFC and PEMFC systems. Energies 2014;7:5502–5522.
579 [16] Tan LJ, Yang C, Zhou N. Performance of the solid oxide fuel cell
580 (SOFC)/proton-exchange membrane fuel cell (PEMFC) hybrid system. Chem Eng
581 Technol 2016;39:689–698.
582 [17] Fernandes A, Woudstra T, van Wijk A, Verhoef L, Aravind PV. Fuel cell electric vehicle
583 as a power plant and SOFC as a natural gas reformer: An exergy analysis of different
584 system designs. Appl Energy 2016;173:13–28.

585 [18] Khan IU, Othman MHD, Hashim H, Matsuura T, Ismail AF, Rezaei-DashtArzhandi M,
586 et al. Biogas as a renewable energy fuel – A review of biogas upgrading, utilization and
587 storage. Energy Convers Manage 2017;150:277–294.
588 [19] Moen OM, Stene HS. Power plant with CO_2 capture based on PSA cycle. Master Thesis,
589 Norwegian University of Science and Technology, Trondheim, Norway, 2014.
590 [20] Lulianelli A, Ribeirinha P, Mendes A, Basile A. Methanol steam reforming for hydrogen
591 generation via conventional and membrane reactors: A review. Renew Sustain Energy
592 Rev 2014;29:355–368.
593 [21] Yang FS, Chen XY, Wu Z, Wang SM, Wang GX, Zhang ZX, et al. Experimental studies
594 on the poisoning properties of a low-plateau hydrogen storage alloy $LaNi_{4.3}Al_{0.7}$ against
595 CO impurities. Int J Hydrogen Energy 2017;42:16225–16234.
596 [22] Wang QD, Wu J, Chen CP, Luo WF, Fang TS. Study on the hydrogen purification
597 technology and apparatus based on metal hydride. Sci Technol Bull Chin 1985;1:1–3.
598 [23] Stiller C, Thorud B, Seljebø S, Mathisen Ø, Karoliussen H, Bolland O. Finite-volume
599 modeling and hybrid-cycle performance of planar and tubular solid oxide fuel cells. J
600 Power Sources 2005;141:227–240.
601 [24] Ni M, Modeling and parametric simulations of solid oxide fuel cells with methane
602 carbon dioxide reforming. Energy Conversion and Management 2013; 70: 116-129.
603 [25] de Groot A. Advanced exergy analysis of high temperature fuel cell systems. Doctoral
604 Thesis, The Energy Research Centre of the Netherlands, Petten, Netherlands, 2004.
605 [26] Aghaie M, Mehrpooya M, Pourfayaz F. Introducing an integrated chemical looping
606 hydrogen production, inherent carbon capture and solid oxide fuel cell biomass fueled

607 power plant process configuration. Energy Convers Manage 2016;124:141–154.
608 [27] Lalik E, Drelinkiewicz A, Kosydar K, Szumełda T, Bielańska E, Groszek D, et al.
609 Oscillatory behavior and anomalous heat evolution in recombination of H_2 and O_2 on
610 Pd-based catalysts. Ind Eng Chem Res 2015;54:7047–7058.
611 [28] Chan SH, Ho HK, Tian Y. Modelling of simple hybrid solid oxide fuel cell and gas
612 turbine power plant. J Power Sources 2002;109:111–120.
613 [29] Massardo AF, Lubelli F. Internal reforming solid oxide fuel cell-gas turbine combined
614 cycles (IRSOFC-GT). Part A. Cell model and cycle thermodynamic analysis. J Eng Gas
615 Turbines Power 2000;122:27–35.
616 [30] Sharma VK, Kumar EA. Effect of measurement parameters on thermodynamic
617 properties of La-based metal hydrides. Int J Hydrogen Energy 2014;39:5888–5898.
618 [31] Jemni A, Nasrallah SB, Lamloumi J. Experimental and theoretical study of a
619 metal-hydrogen reactor. Int J Hydrogen Energy 1999;24:631–644.
620 [32] Chung CA, Lin CS. Prediction of hydrogen desorption performance of Mg_2Ni hydride
621 reactors. Int J Hydrogen Energy 2009;34:9409–9423.
622 [33] Dhaou H, Mellouli S, Askri F, Jemni A, Nasrallah SB. Experimental and numerical study
623 of discharge process of metal hydride beds. Int J Hydrogen Energy 2007;32:1922–1927.
624 [34] van der Lee PEA, Terlaky T, Woudstra T. A new approach to optimizing energy systems.
625 Comput Method Appl M 2001;190:5297–5310.
626 [35] Vera D, de Mena B, Jurado F, Schories G. Study of a downdraft gasifier and gas engine
627 fueled with olive oil industry wastes. Appl Therm Eng 2013;51:119–129.
628 [36] Bagdanavicius A, Jenkins N. Exergy and exergoeconomic analysis of a compressed air

energy storage combined with a district energy system. Energy Convers Manage 2014;77:432–440.

[37] Muhammad U, Imran M, Lee DH, Park BS. Design and experimental investigation of a 1 kW organic Rankine cycle system using R245fa as working fluid for low-grade waste heat recovery from steam. Energy Convers Manage 2015;103:1089–1100.

[38] Marcoberardino GD, Roses L, Manzolini G. Technical assessment of a micro-cogeneration system based on polymer electrolyte membrane fuel cell and fluidized bed autothermal reformer. Appl Energy 2016;162:231–244.

[39] Riensche E, Stimming U, Unverzagt G. Optimization of a 200 kW SOFC cogeneration power plant Part I: Variation of process parameters. J Power Sources 1998;73:251–256.

[40] Lee YD, Ahn KY, Morosuk T, Tsatsaronis G. Exergetic and exergoeconomic evaluation of an SOFC-Engine hybrid power generation system. Energy 2018;145:810–822.

[41] Akkaya AV, Sahin B, Erdem HH. An analysis of SOFC/GT CHP system based on exergetic performance criteria. Int J Hydrogen Energy 2008;33:2566–2577.

[42] Saebea D, Authayanun S, Patcharavorachot Y, Arpornwichanop A. Effects of SOFC exhaust gas recirculation on performance of solid oxide fuel cell-gas turbine hybrid system utilizing renewable fuels. ECS Transactions 2015;68:301–313.

[43] Schlapbach L, Züttel A. Hydrogen-storage materials for mobile applications. Nature 2001;414:353–358.

[44] Zanchini E. A more general exergy function and its application to the definition of exergy efficiency. Energy 2015;87:352–360.